HiSST: 3rd International Conference on
High-Speed Vehicle Science Technology
14 -19 April 2024, Busan, Korea

Numerical Study of the Turbulent Phenomena in Hypersonic Boundary Layers from the Presence of Protuberances and Cavities

Alan Flinton[1], Jim Merrifield[2], William Ivison[3], Matthew McGilvray[4], Frederik Jacobs[5], Johan Steelant[6]

Abstract

The surface of hypersonic vehicles will have small unavoidable surface features as a consequence of the integration of the frame. The impact of these features on the surface heating environment gives rise to key challenges that need to be overcome to allow sustained hypersonic flight. These challenges deserve study due to the turbulent phenomena, i.e. promotion of transition and/or heat flux augmentation. Experiments have been performed in the Oxford High Density Tunnel to characterize the effects caused by such small-scale surface features. This work presents an overview of the numerical analysis undertaken to support these experiments. The agreement between the numerical and experimental data is presented. Highlighted is the possibility of numerical methods to allow for greater parameterization of models in order to support experimental analysis.

Keywords: *hypersonic, gaps, protuberances, transition, heat flux augmentation*

Nomenclature

Latin

h	Height or depth of feature [mm]
IR	Infra-Red
M	Mach number [-]
Re	Reynolds number [-]
St	Stanton number [-]
T	Temperature [K]
TFG	Thin Film Gauge
Tu	Turbulent Intensity [%]
q	Heat flux [W/m^2]
u	Velocity [m/s]
x	Axial distance [m]

Greek

ρ	Density [kg/m^3]

Subscripts

$fence$	Corresponding to "fence" feature
r	Recovery
$step$	Corresponding to "step" feature
$unit$	Unit (Reynolds number)
w	Wall
x	Dimensioned via axial distance
∞	Freestream

1. Introduction

The complex and coupled nature of integrating airframe and propulsion systems for vehicles designed for sustained hypersonic flight is very well acknowledged [1] [2]. However, the integration challenges associated with steps and gaps that have to be introduced into the design for practical manufacturing reasons have received less attention yet have high significance [3]. These challenges deserve study

[1] *Fluid Gravity Engineering Ltd., 1 West Street, Emsworth, PO10 7DX, UK, alan.flinton@fluidgravity.co.uk*
[2] *Fluid Gravity Engineering Ltd., 1 West Street, Emsworth, PO10 7DX, UK, alan.flinton@fluidgravity.co.uk*
[3] Oxford Thermofluids Institute, *University of Oxford, Southwell Building, Osney Mead, Oxford, OX2 OES, UK*
[4] Oxford Thermofluids Institute, *University of Oxford, Southwell Building, Osney Mead, Oxford, OX2 OES, UK*
[5] *ESA ESTEC, Keplerlaan 1, 2201 AZ Noordwijk, Netherlands*
[6] *ESA ESTEC, Keplerlaan 1, 2201 AZ Noordwijk, Netherlands*

due to the turbulent phenomena, i.e. promotion of transition and/or heat flux augmentation, that such features can introduce. Thermal management is often a key design driver for hypersonic vehicles and as such it is beneficial for design and integration activities to have access to engineering-level methods and tools that can predict the effect that features such as gaps and protuberances have on heat fluxes. Detailed in this study are numerical investigations which are part of a wider effort to eventually provide a robust and rapid capability for design engineers to take account of these features. Modelling efforts follow two main avenues:

- Navier-Stokes simulations to help set test conditions from experiments, interpret test data, and establish the reliability of commonly applied modelling techniques (reported here).
- Development of engineering-level methods to directly assist the design process based on the Navier-Stokes simulations and experimental output. This tool is described in more detail by Jacobs *et al.* [4]; initial and subsequent development is described by Hoffmann et al. [5] Karsh et al. [6]

This paper details the numerical rebuilding activities performed on vehicle-relevant wind tunnel experiments at Oxford's High-Density Tunnel (HDT) facility. Two phases of testing were performed and are detailed herein.

1. Quantifying effect of features - An initial phase of testing looking at the effect of features (steps, cavities, backward-facing steps) on the transition of hypersonic boundary layers. Several flow conditions were explored.
2. Turbulent heat flux augmentation – The second phase focused on the impact of features on an already turbulent boundary layer. That is flow conditions were selected that enforced transition prior to the feature.

2. Experimental Setup

2.1. HDT Overview

Experiments were carried out at the Oxford HDT (High Density Tunnel) facility, shown in Fig 1. Nozzles exist for Mach numbers 4, 5, 6, and 7 which can be interchanged as needed. The HDT typically operates as a Ludwieg tunnel producing periods of steady flow between 30 and 50 ms depending on the condition. In addition to Ludwieg mode, a piston stroke can be incorporated into the firing sequence to further heat the test gas, referred to as LICH (Light Isentropic Compression Heating) [7]. For further details on the construction and operation of the HDT, see McGilvray [8] and Wylie [9].

Fig 1. The Oxford High Density Tunnel (HDT)

2.2. Test Article

The HDT test section, with instrumentation annotated, is shown in Fig 2. The section in general is a sharp flat plate, 575 mm in length and 300 mm in width. The upper surface of the model consists of two independently actuated blocks, allowing features of interest to be set. The first, an "upstream fence" is located at an axial position of 150 mm and is 5 mm in running length and 140 mm in width. The second section is a "downstream step plate" which is located at an axial position of 155 mm (immediately downstream of the "upstream fence") and is 390 mm in running length and 110 mm in width. Fig 2 shows the main features of interest examined numerically within this paper. Note that more combinations were experimentally analysed and are reported by Ivison *et al.* [10].

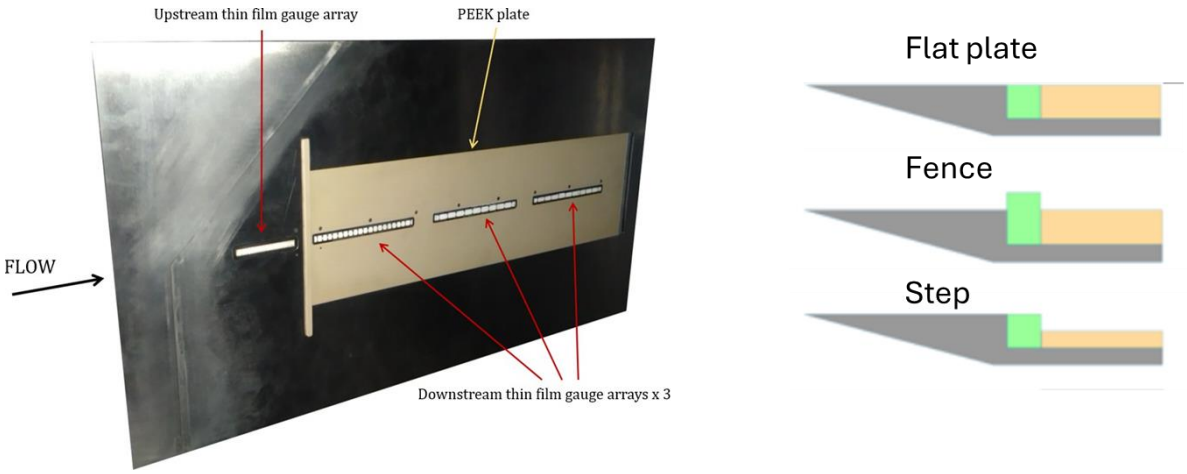

Fig 2. Experimental model with instrumentation annotated (left) example geometries of interest (not to scale) (right)

2.3. Measurement techniques

Two measurement techniques were primarily used within the HDT to assess the level of heat flux on the surface of the geometry of interest; IR (Infra-Red) thermography and Thin Film Gauges (TFG). Both sources were used as a source of comparison towards the numerical results.

The first phase of work (quantifying effect of features) primarily used TFGs for comparison to numerical data due to the IR measurement system being in its infancy during this period of testing.

For the turbulent augmentation phase of work, the IR results are treated as the main data source, with TFGs used to confirm that the boundary layer state at their location (i.e. has transition occurred).

For further details on measurement techniques and calibration see Ivison et al. [10]

3. Run Conditions

The following subsections report the run conditions for the two experimental phases.

3.1. Quantifying effect of features

Various cases were explored within the first phase of work. This was to explore the effect of the conditions on the transition location and the subsequent impact of the features of interest. Table 1 details the conditions explored. Numerically the conditions termed Nominal and LICHA are equivalent; it is only the method of wind tunnel operation changing. Within the numerical analysis only condition LICHA will be reported.

The nominal condition refers to a historic condition, M5A, M5B, and M5C corresponding to the facility running in Ludwieg mode. Across these conditions T_r/T_w is kept constant with the Reynolds number varied. The LICH conditions correspond to the facility being run in LICH mode with varying Reynolds numbers explored with T_r/T_w kept constant between conditions.

The main features of interest during this phase of work were that of a 1.5 mm high fence of length 5 mm and a 1.5 mm deep cavity of length 5 mm. For this phase of work, the actuators described in Section 2.2 were not yet developed.

3.2. Turbulent Heat Flux Augmentation

The second phase of work focused on exploring the impact of the features within a turbulent boundary layer. Subsequently, freestream conditions were selected in order to enforce transition on a flat plate prior to the feature.

Conditions for the cases of interest are given in Table 2. Shot 3055 was a flat plate case with a sharp leading edge undertaken to provide a baseline to the cases with features present. The features were set using the actuators described in Section 2.2. Shots 3056 and 3057 explored the influence of 1 mm and 2 mm high fences respectively, and Shots 3034 and 3040 explored the influence of 1 mm and 2 mm deep backward-facing steps respectively.

The final two shots, 3189 and 3187 explored the impact of leading-edge radius on transition location. Note that these two cases were undertaken at a Mach number of 7.2, preventing direct comparison to the other cases.

Table 1. Run conditions for quantifying effect of features

Condition	M_∞	Re_{unit}	u_∞	ρ_∞	T_∞
[-]	[K]	[/m]	[m/s]	[kg/m^3]	[K]
Nominal	6	3.96E+07	891.0	0.1544	54.9
M5A	5	3.50E+07	864.3	0.2159	74.4
M5B	5	3.86E+07	864.3	0.2382	74.4
M5C	5	2.33E+07	864.3	0.1439	74.4
LICHA	6	3.96E+07	891.0	0.1544	54.9
LICHB	6	0.91E+07	891.0	0.0402	54.9
LICHC	6	0.91E+07	1260.0	0.0512	109.8
LICHD	6	1.36E+07	1260.0	0.07721	109.8

Table 2. Run conditions for shots exploring turbulent heat flux augmentation

Shot ID	T_∞	u_∞	ρ_∞	Re_{unit}	M_∞	r_{LE}	h_{fence}	h_{step}
[-]	[K]	[m/s]	[kg/m^3]	[/m]	[-]	[mm]	[mm]	[mm]
3055	51.1	893.5	1.00E-01	2.49E+07	6.1	0.00	0.00	0.00
3056	51.2	894.2	1.00E-01	2.49E+07	6.1	0.00	1.00	0.00
3057	51.8	897.1	1.01E-01	2.48E+07	6.1	0.00	2.00	0.00
3034	51.2	895.0	1.00E-01	2.49E+07	6.1	0.00	0.00	-1.00
3040	50.7	889.6	1.02E-01	2.55E+07	6.1	0.00	0.00	-2.00
3189	38.9	911.6	7.59E-02	2.52E+07	7.2	0.00	0.00	0.00
3187	39.9	923.1	7.42E-02	2.44E+07	7.2	0.05	0.00	0.00

4. Numerical Setup

4.1. Setup

Fluid Gravity's in-house CFD solvers, TINA and ANITA were used to conduct the numerical analysis. TINA [11] was used to conduct the simulations corresponding to the first phase of analysis. ANITA [12] was used to conduct the simulations corresponding to the second phase of analysis. TINA is a finite-volume CFD code that solves the Navier-Stokes equation using models for thermal and chemical non-equilibrium with finite reaction rates. TINA requires a structured mesh, whereas ANITA solvers the same conservation equations but can take arbitrary unstructured mesh as input. This, together with the modernized input format of ANITA led to a reduction in the setup time of the cases, particularly when meshing (see Section 4.2 for more information on meshing). ANITA was under development during the first phase of analysis with respect to the capabilities of interest and as such was not used from kick-off.

2D simulations were undertaken unless otherwise noted. The HLLC flux scheme [13] was taken for use, within ANITA and solutions with second order spatial accuracy were achieved.

The SST Transitional turbulence model from Langtry and Menter [14] [15] was taken for use. The turbulence model was typically switched on at a later time in the simulation (20,000) steps to allow the flow within the domain to establish before turbulence is introduced. This was found to improve stability. The freestream turbulent intensity, Tu_∞, of the flow was varied prior to conducting the bulk of the simulations in order to determine which value gave the best match to experimental data. This value was then taken forward for use when analysing all subsequent cases of interest. This is reported in Section 5.1. Through selecting the SST turbulence model for use it is hoped that the results will compare favourably to experimental measurements. The SST model is selected over more computationally intensive methodologies, such as DNS, to allow scope for quick parametric analysis in future work.

Analysis corresponding to the first phase had two gas species present, Oxygen and Nitrogen, for which the mass fractions were set at 23 % and 77 % respectively. For the second phase of analysis the working gas was 100 % Nitrogen.

Low-temperature Blottner viscosity coefficients [16] were taken for use. High-temperature coefficients, commonly employed in hypersonic solvers will be less accurate at the low temperatures of interest. A comparison of viscosity determined by using the high-temperature Blottner coefficients, low-temperature coefficients and Sutherland and Keyes coefficient is shown in Fig 3. It is clear that the low-temperature Blottner coefficients align much better with the Sutherland and Keyes data. Taking shot 3189 as a baseline, the change in predicted transition location was not insignificant, at approximately 120 mm.

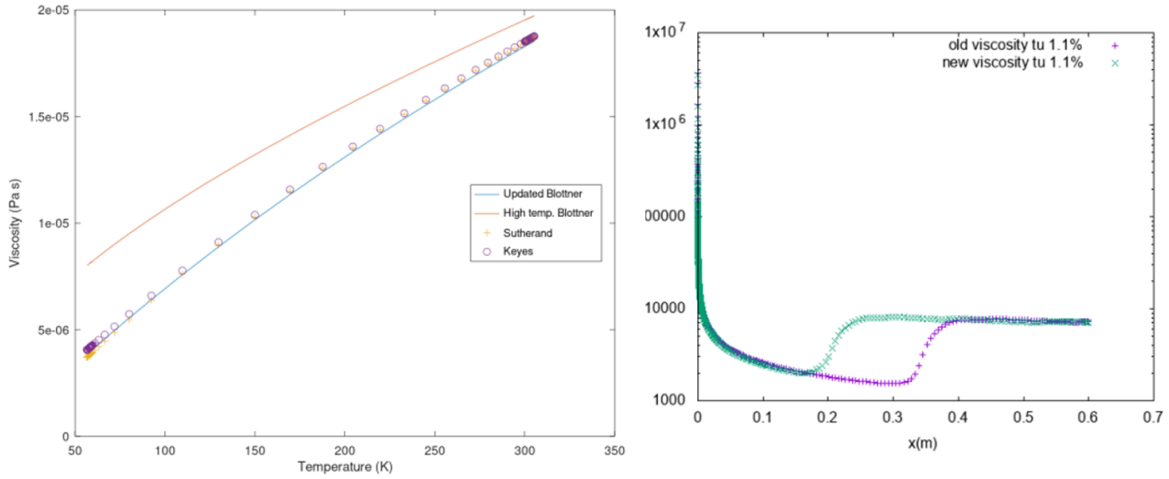

Fig 3. Left: Comparison of viscosity models; Right: Impact on transition location (scoping case)

The experiments were modelled using 2D planar simulations. The wall boundary was set as an isothermal wall at 300 K. It was, therefore, assumed that the model was perfectly aligned with a parallel freestream. As such, possible 3D effects were ignored for 2D simulations.

It was assumed that the model's leading edge was perfectly sharp unless otherwise noted. In reality, the model's finite radius, albeit very small (< 0.01 mm) will influence boundary layer growth which could in principle affect transition characteristics. The influence of a blunt leading edge was explored within this study. Shot 3187 was undertaken with a leading edge of 0.05 mm.

4.2. Mesh Construction

The meshes for numerical analysis were constructed using Pointwise [17]. For all cases, the maximum cell spacing along the wall was limited to 1 mm. Through mesh refinement this was found to minimize the impact of the mesh of the predicted transition location. The wall spacing normal to the wall was set to 1×10^{-6} m.

The domain height had to be high enough to capture the weak shock impinging of the leading edge of the plate as well as any introduced through features. As a result, the height of the domain increases with axial distance. Mesh independence was achieved for all cases and is reported in Section 5.1.

As TINA was used for the first phase of analysis, the meshes used had to be structured. Shown in Fig 4 are the resultant meshes for the fence and cavity. The resultant cell-count for the meshes was 52,000 for the flat plate and 139,329 for both the fence and cavity.

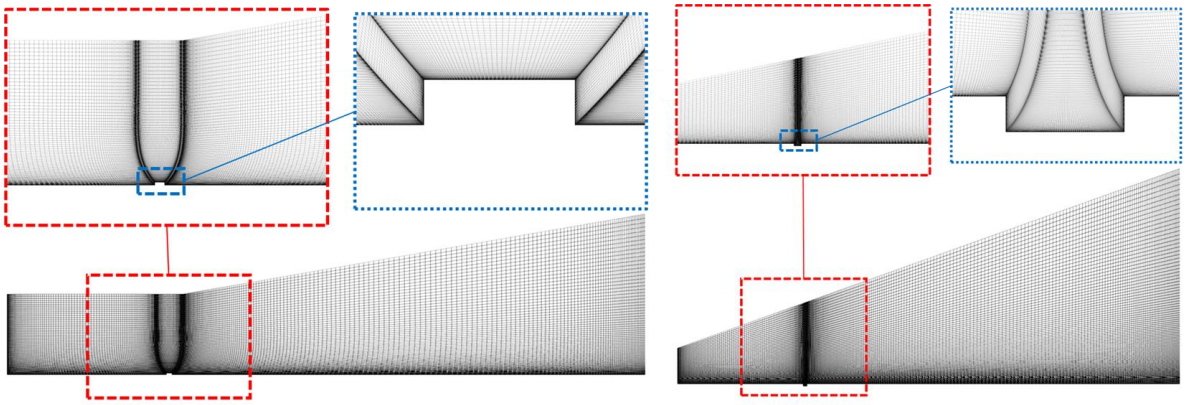

Fig 4. First phase structured meshes; Left: 1.5 mm high fence; Right: 1.5 mm deep cavity

For the second phase of analysis unstructured meshes were constructed. An unstructured domain was found to greatly decrease the run time of the cases compared to structured meshes. Areas of cell refinement could target locations where gradients are expected to be high, such as around the geometries of interest. It can be seen for the unstructured meshes (Fig 4) that these refinement regions extend out towards the freestream, resulting in high cell concentrations in areas of little interest.

For all unstructured meshes a baffle region was constructed in the freestream just below the top boundary, this was found to aid in the stability of the numerical solution.

The mesh corresponding to the sharp leading-edge case is shown in Fig 5. Also shown in Fig 5 are the step and backwards facing meshes. The cell counts were 43726, 99027, 101283, 47515 and 51324, for the flat plate, 1 mm fence, 2 mm fence, 1 mm step and 2 mm step respectively.

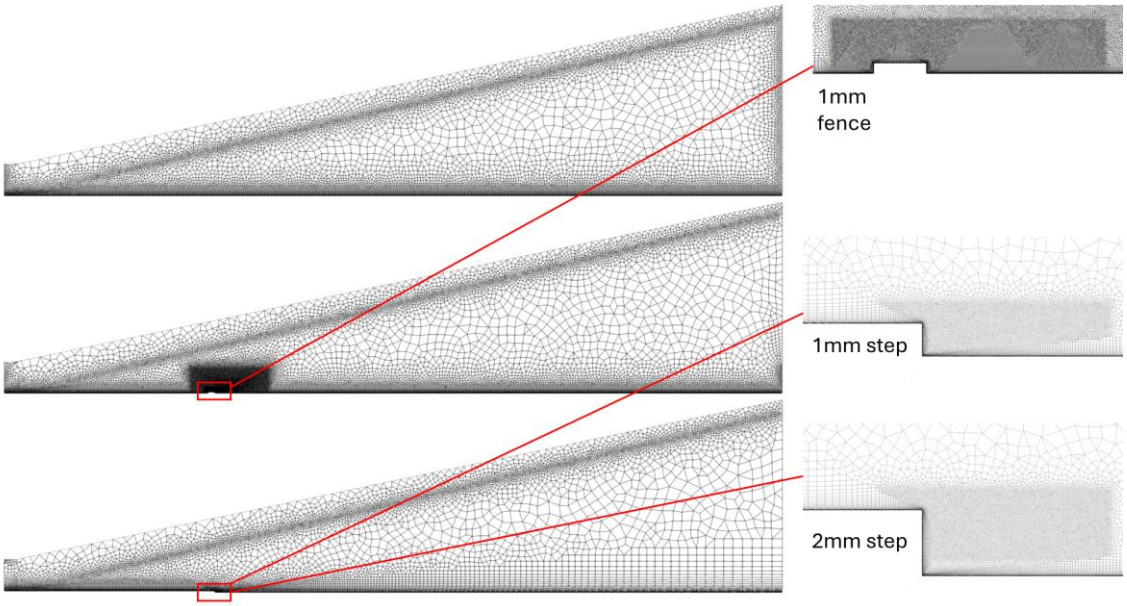

Fig 5. ANITA unstructured meshes; top: flat plate, middle: 1 mm fence, bottom: 1 mm step (with 2mm step shown in instep)

Only a flat plate case was of interest for the blunt leading edge. As a result, a 2D structured mesh was constructed, as shown in Fig 6. Note high levels of mesh refinement were required in order to achieve

mesh convergence. The total cell count is 77,213 cells with the wall spacing set to 1×10^{-6} m and the clustering towards the nose set to 5×10^{-7}m.

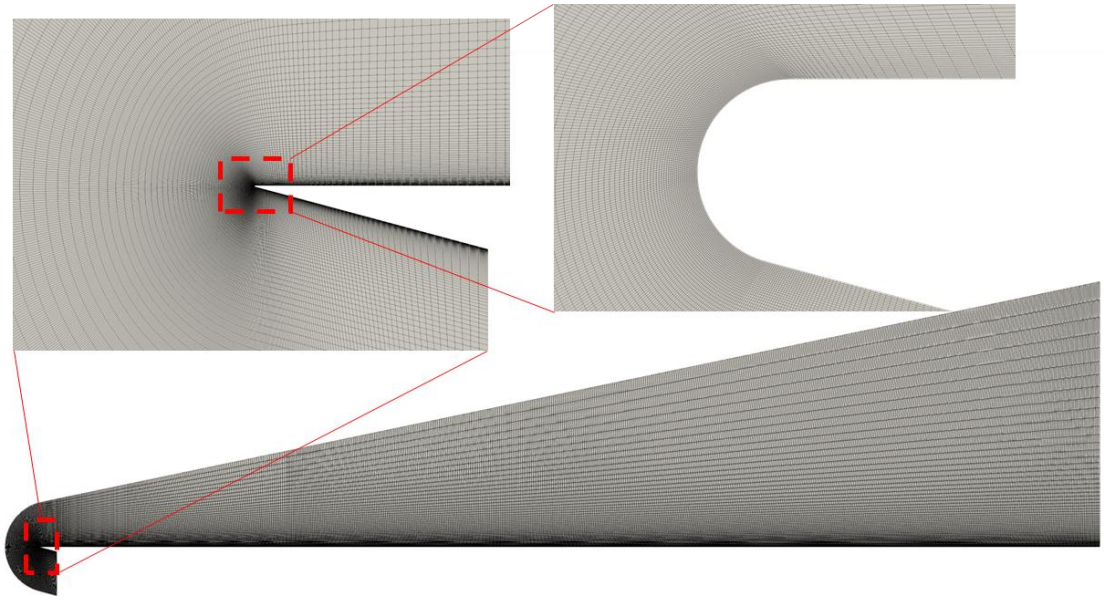

Fig 6. Blunt leading edge mesh

5. Results – quantifying effects of features

5.1. Establishment of baseline conditions

Preliminary runs were undertaken to determine the level of freestream turbulent intensity, Tu_∞, required to match the experimental results. Experimental results through TFG were available for the LICHA condition. A freestream value of 0.77 % was found to match the experimental transition region well and taken for use. The results from this iterative process are shown in Fig 7, along with the mesh resolution study for the three levels of mesh outlined in Section 4.2.

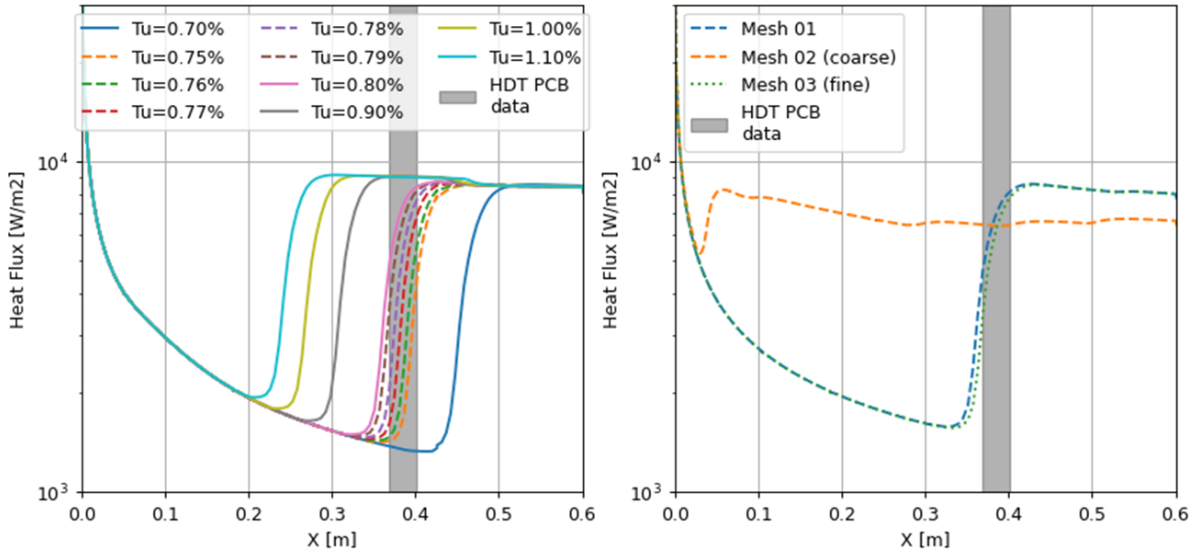

Fig 7. Left: iteration of Tu_∞; Right: mesh convergence results

5.2. Flat Plate Analysis

Heat flux versus axial distance and Stanton number versus unit Reynolds number are presented in Fig 8.

Compared to the baseline LICHA case, the M5A case predicts earlier transition. The unit Reynolds number and recovery temperature ratio were configured to be comparable across the two cases. However, the Mach number for the M5A case is lower, 5, compared to that of the nominal case, 6. As a result for M5A the freestream velocity decreased, and the freestream density and temperature increased marginally to compensate. It is thought that lowering the Mach number will lead to an earlier transition compared to the nominal case as increasing the Mach number generally increases the stability of the boundary layer above edge Mach numbers of 4.

The aim of the M5B case was to maintain the T_r/T_w value with respect to the M5A case and increase the freestream unit Reynolds number. The higher Reynolds number leads to an earlier transition. The constant T_r/T_w parameter leads to the heat flux values for the M5B and M5A cases being relatively comparable.

The M5C case parameters were set to have the same T_r/T_w as the LICHA condition but with a lower unit Reynolds number studied. It would be expected that the lower unit Reynolds number would lead to delayed transition compared to the nominal case and that heat fluxes between the two cases remain comparable. Through inspection of Fig 8 this is shown to be the case.

No transition is predicted to occur at the LICHB, LICHC and LICHD, primarily due to the low unit Reynolds number of the conditions.

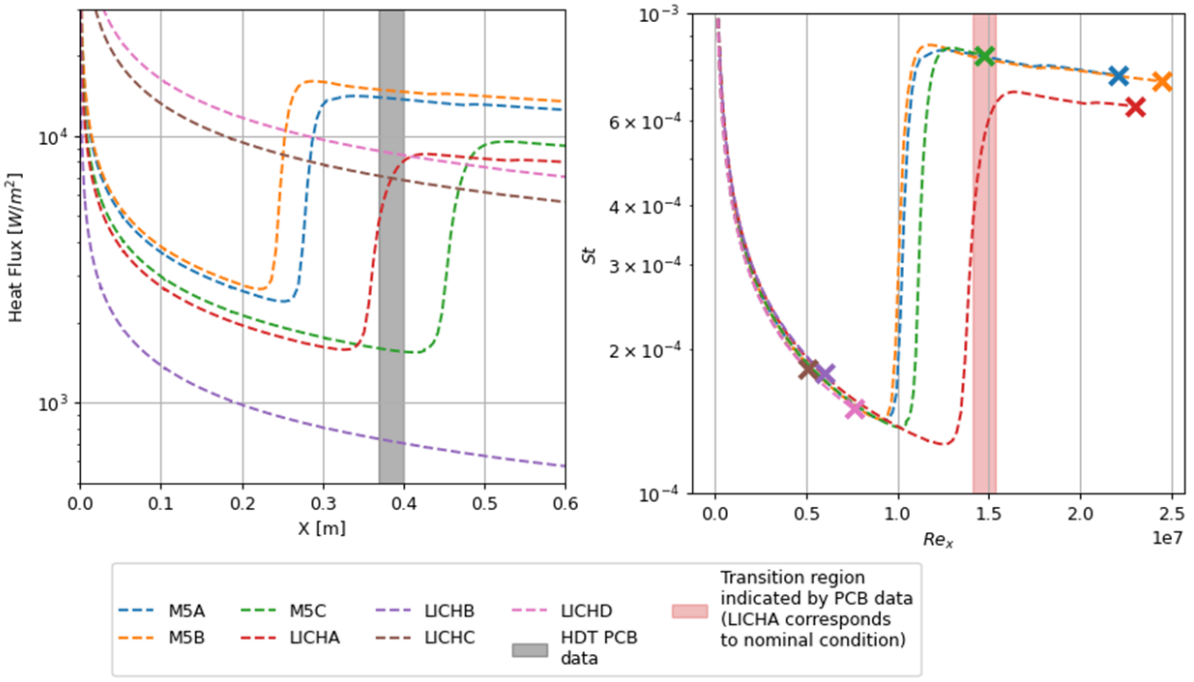

Fig 8. Flat plate results; Left: Heat flux versus axial distance; Right: Stanton number versus unit Reynolds number

5.3. Feature Impact Analysis

Shown in Fig 9 is heat flux versus axial distance for two cases, LICHA and M5A, Table 3 reports the results for the rest of the conditions.

Both protuberance cases shown predict transition immediately aft of the feature, as such they are predicted to disturb the boundary layer to such an extent that recovery is not possible. Immediately prior to the protuberance a drop in heat flux is predicted, this is due to the separation of the flow, highlighted in Fig 10.

For the M5A case the presence of the cavity is sufficient to cause the boundary layer to transition to the turbulent regime aft of the feature. For the LICHA case this is not the case, a local increase in heat flux is predicted, but then the boundary layer recovers to laminar values of heat flux before transitioning at a similar point to the corresponding flat plate. As mentioned for the flat plate cases this is likely due to the increased Mach number of the LICHA case leading to a favourable pressure gradient within the

boundary layer. Shown in Fig 11 is the local cavity flow regime along with the reported surface heat flux. Although values are lower, they are not inconsequential and still of interest from a design perspective, indeed the lower heat flux values could be useful for components which require a view to the outside.

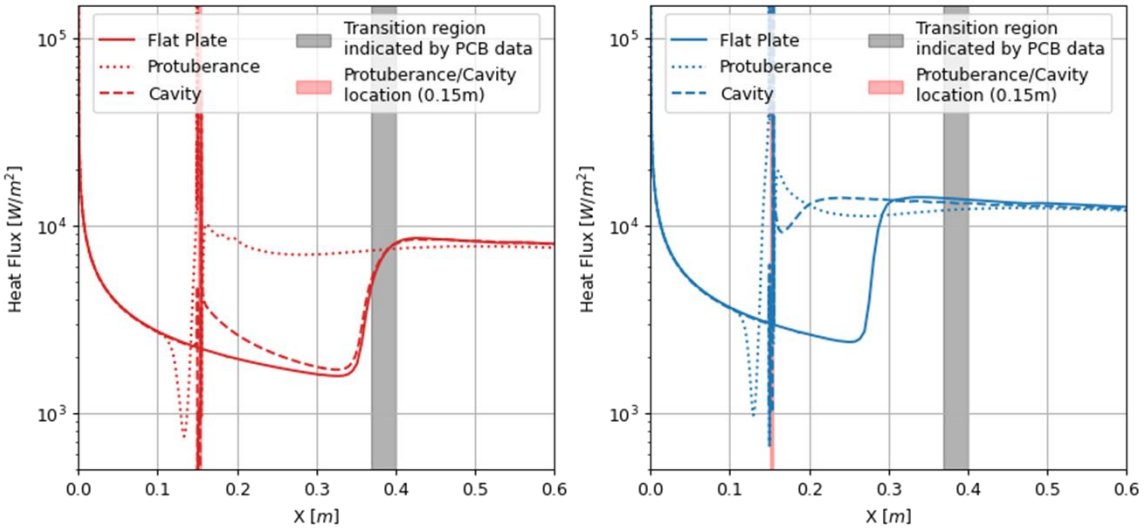

Fig 9. Heat flux versus axial distance; Left: LICHA; Right: M5A

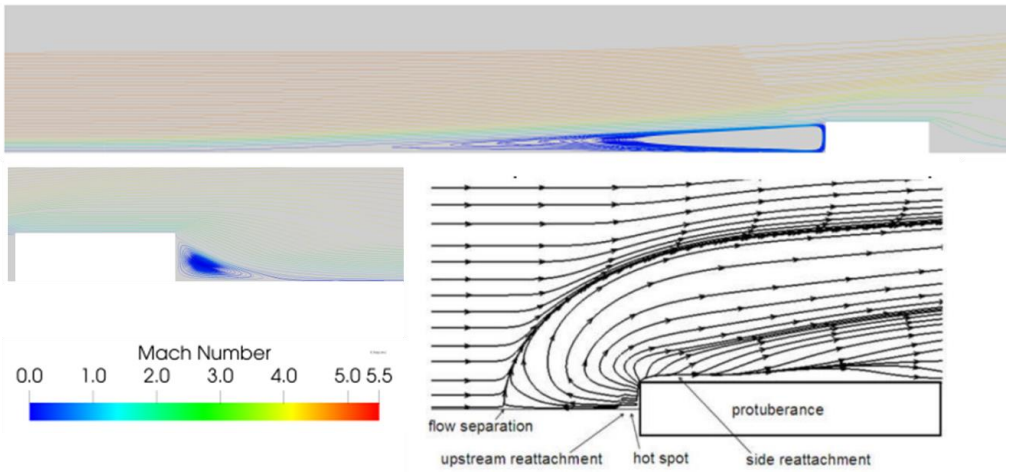

Fig 10. Protuberance local flow field for LICHA case. Clockwise from top: 1) Focus on upstream separation region 2) Protuberance features taken from [18] 3) Focus on aft separation region

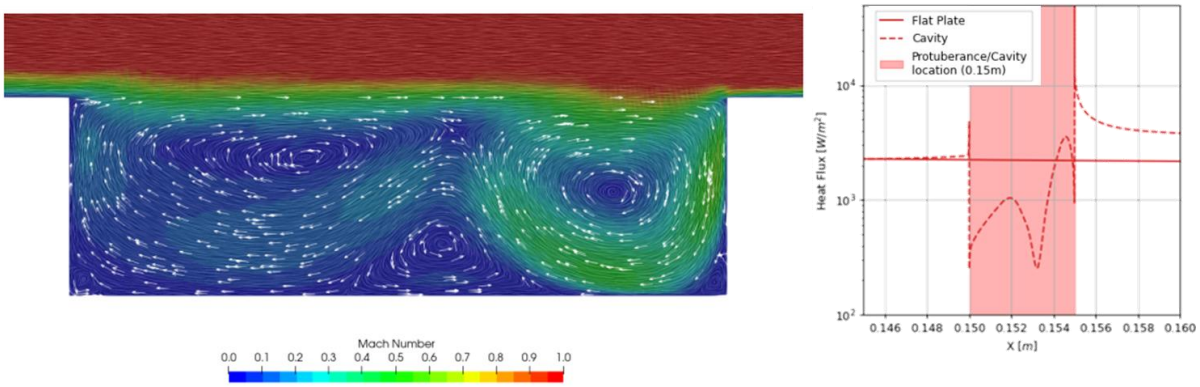

Fig 11. Cavity local flow field for LICHA case; Left: Streamlines showing recirculation regions within cavity; Right: Heat flux across cavity

Table 3. Effects of protuberance and cavity on predicted transition location for Phase 1 conditions

Condition	M_∞	Re_{unit}	T_r/T_w	Predicted Transition Location		
				Flat Plate	**1 mm fence**	**1 mm cavity**
[-]	[K]	[/m]	[-]	[m]	[m]	[m]
M5A	5	3.50E+07	1.329	~ 0.28	~ 0.155 (immediately aft of feature)	~ 0.155 (immediately aft of feature)
M5B	5	3.86E+07	1.329	~ 0.25	~ 0.155 (immediately aft of feature)	~ 0.155 (immediately aft of feature)
M5C	5	2.33E+07	1.329	~ 0.48	~ 0.155 (immediately aft of feature)	~0.400 (intermittent aft of feature)
LICHA	6	3.96E+07	1.329	~ 0.39	~ 0.155 (immediately aft of feature)	~0.39 (same as flat plate, intermittent aft of feature)
LICHB	6	0.91E+07	1.329	No transition	~ 0.155 (immediately aft of feature)	~ 0.155 (immediately aft of feature)
LICHC	6	0.91E+07	2.658	No transition	~ 0.5 m fully turbulent Intermittent aft of feature	~ 0.155 (immediately aft of feature)
LICHD	6	1.36E+07	2.658	No transition	~ 0.155 (immediately aft of feature)	Intermittent BL aft of feature, recovers to laminar

6. Results – turbulent heat flux augmentation

6.1. Baseline flat plate

The baseline flat plate result, shot 3055, shown in Fig 12. The value of Tu_∞ was set to 2 % for all ANITA cases presented in for this phase of study. This value allowed the experimental transition location to be well mated, occurring between 100 and 150 mm. Good agreement is shown between the numerical and experimental turbulent heat flux magnitude.

The numerical turbulent flat plate case will be used to calculate the normalised heat flux presented later in this section for various cases, as per the equation below:

$$q_{ref} = \frac{q_{transitionalCase}}{q_{flatPlateTurbulent}}$$

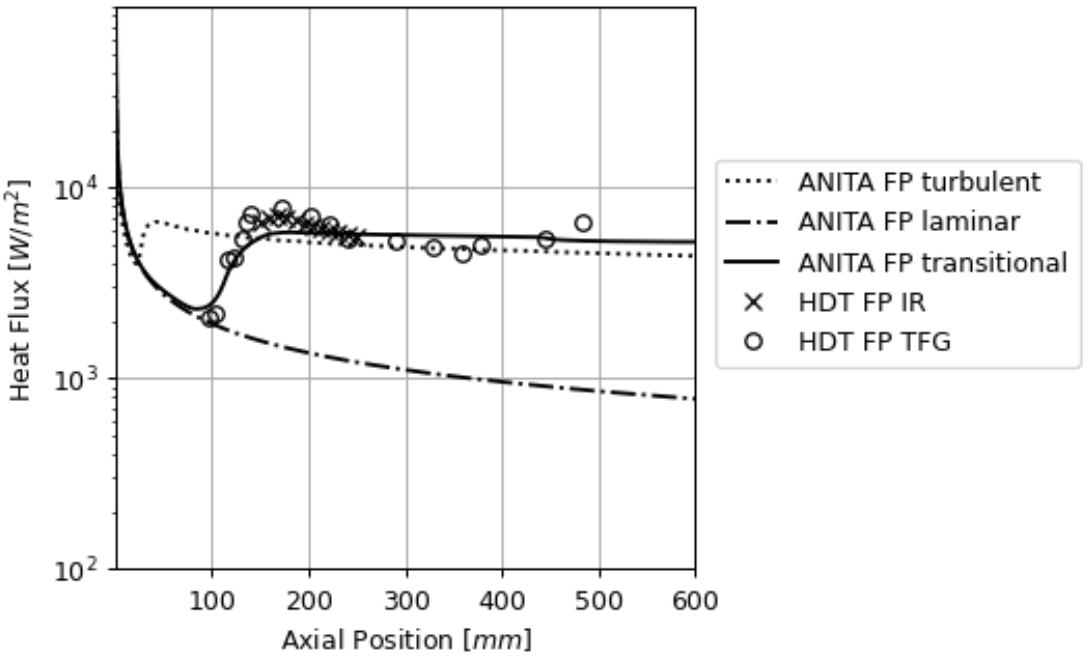

Fig 12. Turbulent augmentation (Ma 6) sharp flat plate analysis

6.2. Fence turbulent heat flux augmentation

The heat flux and normalized heat flux for the 1 mm and 2 mm (shots 3056 and 3057) cases are shown in Fig 13 and Fig 14 respectively. The transition location is similar to that of the flat plate case, indicating that the presence of the fence has a negligible effect on the onset of transition prior to the feature.

The magnitude of heat flux augmentation for the 1 mm fence case shows a very good agreement between the numerical and experimental cases for the first 30 mm aft of the feature. Beyond this the results deviate, with the experimental value tending back towards unity, and the numerical result drifting away from unity, as shown for the corresponding heat flux plot the transitional value of heat flux remains below that of the turbulent flat plate case. This indicates that the numerical method presented can be used to extend the experimental methodology to additional geometries of interest.

The 2 mm fence case matches the location of the experimental peaks well. However, the magnitude is not matched as well as the 1 mm case. The experimental heat flux augmentation between the 1 mm and 2 mm cases remains approximately constant, at around 1.25. The numerical results suggest an increase from 1.20 to 1.75 in normalized heat flux. 3D effects could possibly be more dominant for the 2 mm step, these will not be accounted for in the numerical cases and could explain the discrepancy.

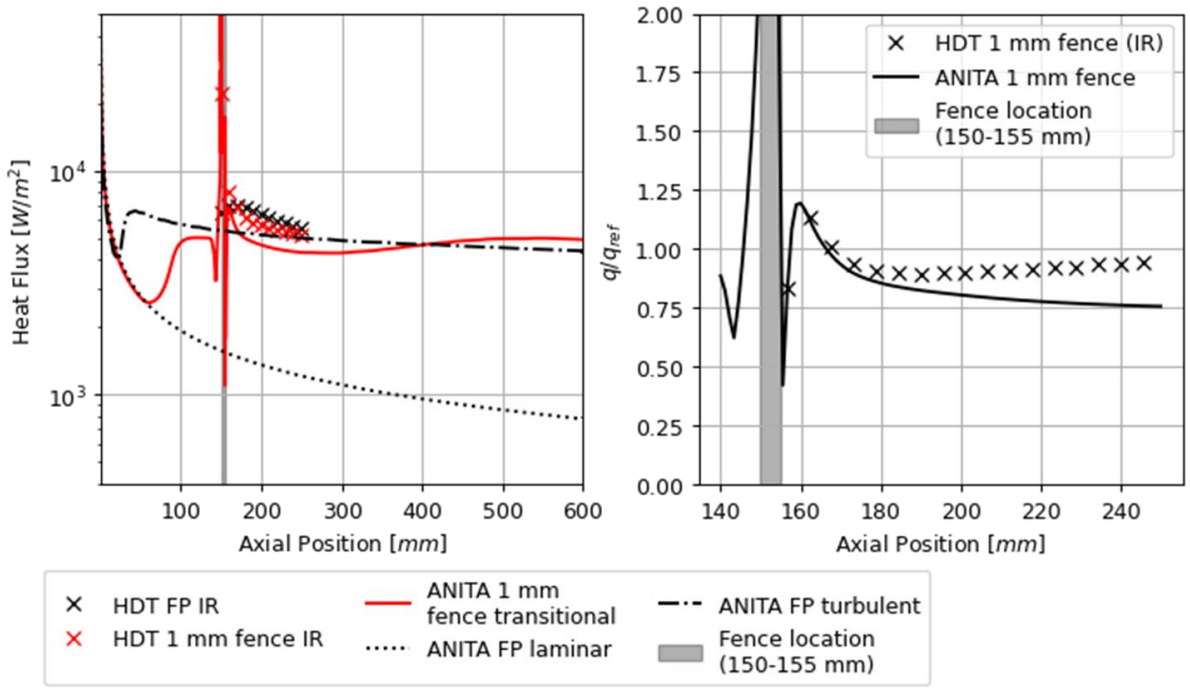

Fig 13. 1 mm fence numerical versus experimental comparison; Left: Heat flux; Right: normalised heat flux

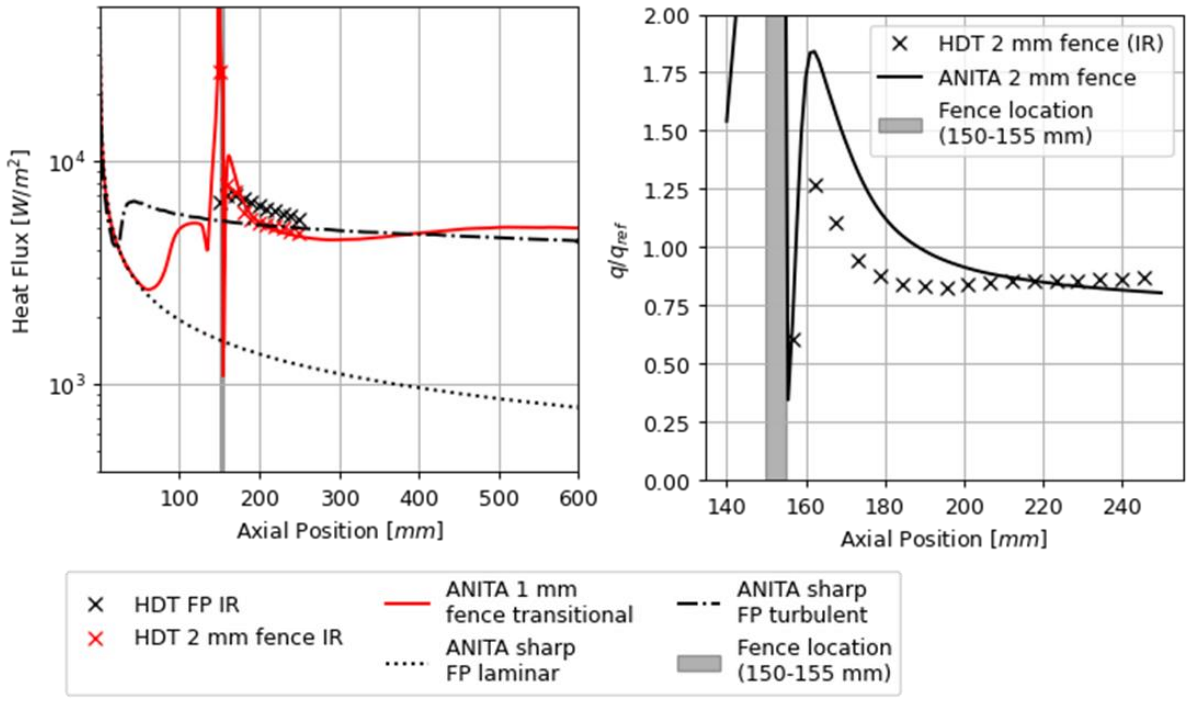

Fig 14. 2 mm fence numerical versus experimental comparison. Left: Heat flux; Right: normalised heat flux

6.3. Backward facing step turbulent flux augmentation

The results for the two backward facing step cases simulated (shot 3034 and 3040) are shown in Fig 15 and Fig 16 for the 1 mm and 2 mm step respectively. As with the fence cases the onset of transition is not altered by the presence of the feature. The trough of peak flux augmentation aft of the steps is significantly lower than that reported experimentally. This is a numerical artifact due to the shaded cells at the corner of the step being isolated from the flow. Beyond this region the profile numerical result deviates from the experimental IR data. A small plateau is seen just after 160 mm, this is likely due to

an extension of the recirculation region aft of the plate. As with the fence cases, beyond 240 mm the transitional case heat flux remains below the turbulent flat plate case. The level of augmentation reported numerically is minimal, as a result the application of the numerical method for the step cases is not as promising compared to the two previously reported fence cases.

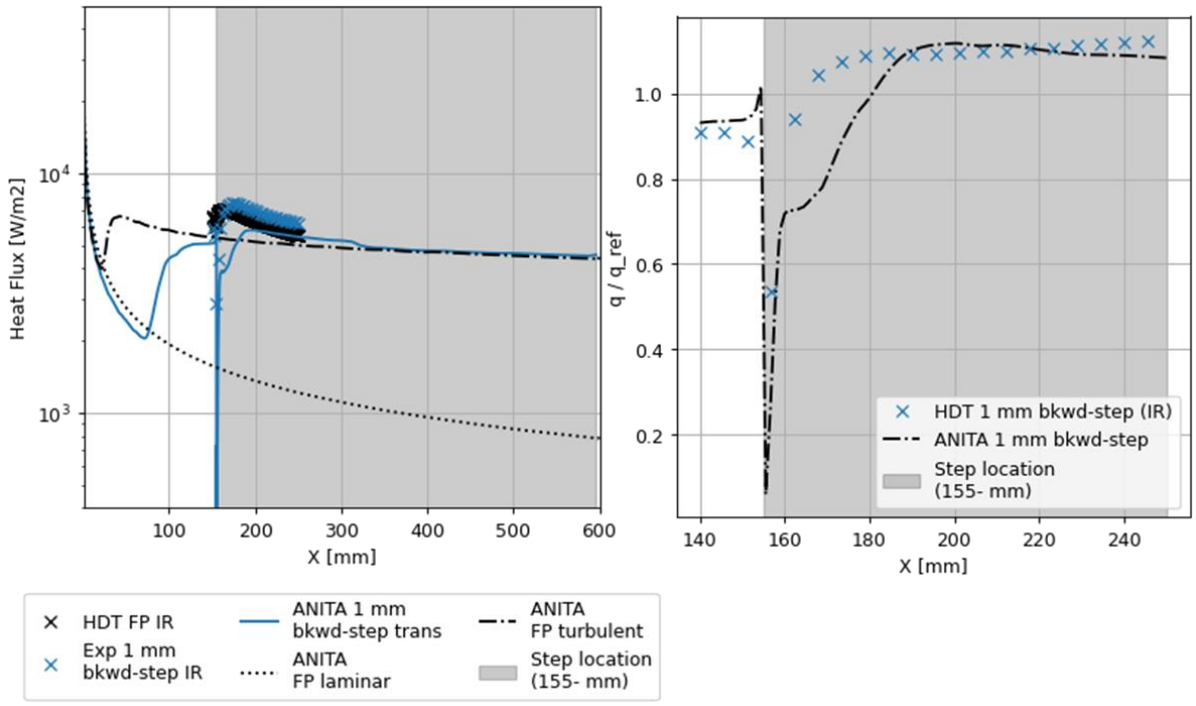

Fig 15. 1 mm backward facing step numerical versus experimental comparison. Left: Heat flux; Right: normalised heat flux

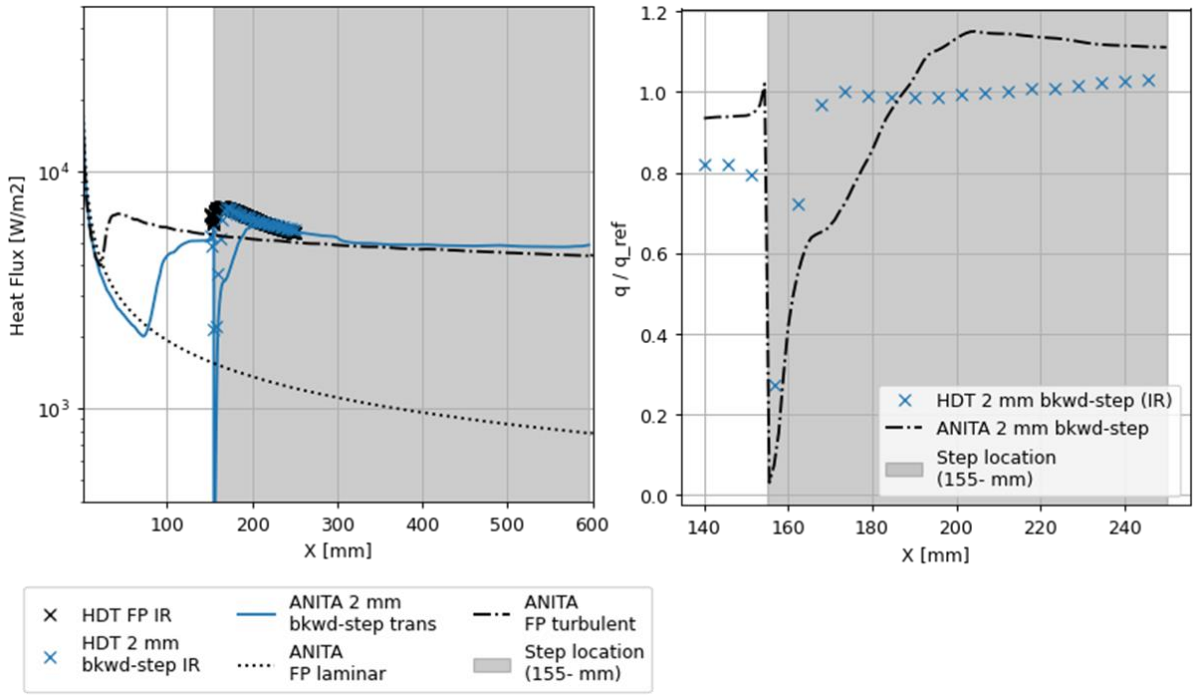

Fig 16. 2 mm backward facing step numerical versus experimental comparison. Left: Heat flux; Right: normalised heat flux

6.4. Sharp versus blunt leading edge

Shot 3189 and 3187 were consistent except with the leading-edge radius of the flat plate. Fig 17 presents the resultant heat flux along the plate predicted for the two cases. Both cases show good agreement with the experimental laminar data, the values of for turbulent heat flux predicted are slightly below that recorded experimentally.

The sharp case is shown to match the experimental transition location well, at approximately 150 mm, giving confidence in the results. The introduction of a blunt leading edge was found to push the transition location back by approximately 200 mm to 350 mm for the numerical case. This is slightly lower than the deviation reported experimentally, but nonetheless the phenomena is captured. This finding is of interest due to the subsequent delay in the transition. Typically delaying transition is beneficial on the surface of hypersonic vehicles. This result suggests that rounding sharp edges marginally could lead to an extra 20 cm of laminar flow, depending on the total length of the vehicle this may be worth the benefit of inclusion.

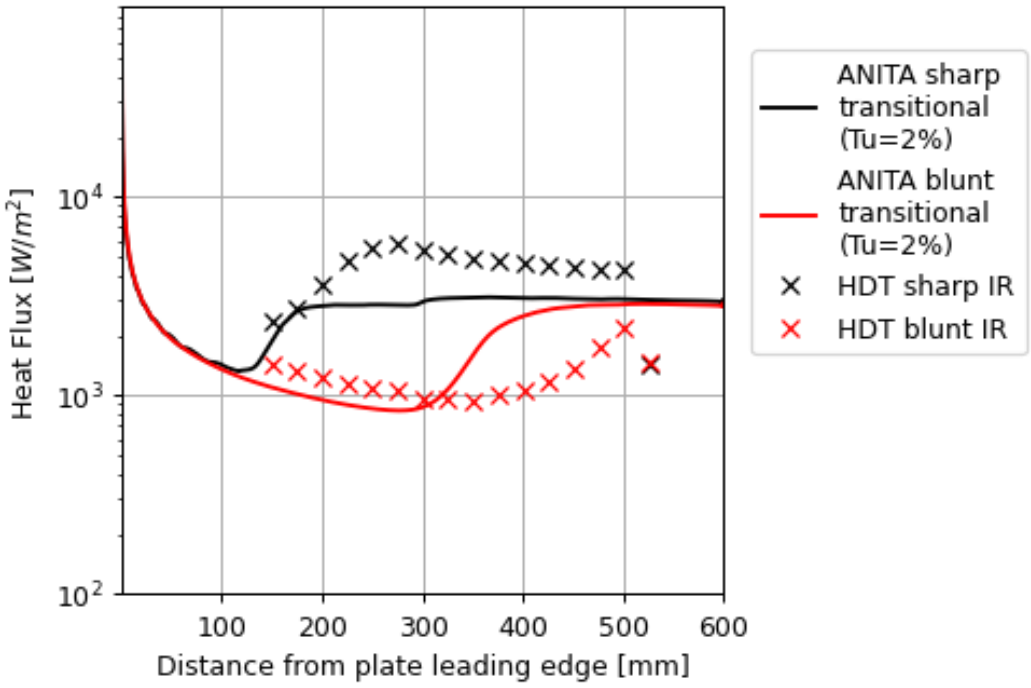

Fig 17. Impact of blunt leading edge on transition location

7. Conclusions

Numerical analysis has been shown to be valuable in quantifying the effects of features within a hypersonic boundary layer with respect to the onset of transition. When assessing turbulent heat flux augmentation numerical analysis was shown to give a good match when considering fences of height 1 and 2 mm. It would be of interest in future work to extend the analysis to develop a parametric dataset for varying fence heights and lengths. Poorer agreement was shown for the backward facing step cases, with little turbulent heat flux augmentation being predicted numerically. Overall agreement with experiment is very encouraging given the Reynolds averaged approach of the numerical method employed and shows that industrially accessible turbulence modelling has some utility when investigating the effect of gaps, cavities and protuberances although this approach is still likely to be less generally applicable than unsteady, hybrid or DNS analysis.

Acknowledgements

Thanks to ESA for funding this work through contract 4000129548/19/NL/BJ/ig.

References

[1] S. A. Berry, T. J. Horvath, F. A. Greene, G. R. Kinder and K. C. Wang, "Overview of Boundary Layer Transition Research in Support of Orbiter Return to Flight," AIAA Paper 2006-2918, 2006.

[2] J. Steelant, "Evolutionary technology developments towards an international flight platform for high-speed transportation, aviation in Europe Innovating for Growth," in *Proceedings of the 7th European Aeronautics Days*, London, UK, 2015.

[3] N. Sandham and J. Van den Eynde, "Outcome of high-speed boundary layer transition workshop at HiSST 2022," *CEAS Space Journal,* May 2023, doi: 10.1007/s12567-023-00503-1.

[4] F. Jacobs and J. Steelant, "A Boundary Layer Analysis on the HEXAFLY-INT Experimental Flight Test Vehicle," in *HiSST: 3rd International Conference on High-Speed Vehicle Science & Technology*, Busan, Korea, 2024, HiSST_2024-0029.

[5] J. P. Hoffmann, J. van den Eynde and J. Steelant, "An analysis tool for boundary layer and correlation-based transition onset assessment on generic geometries," *CEAS Space Journal,* 2023, doi: 10.1007/s12567-023-00507-x.

[6] M. Karsch, J. van den Eynde and J. Steelant, "Linearly combined transition model based on empirical spot growth correlations," *CEAS Space Journal,* 2023, doi: 10.1007/s12567-023-00499-8.

[7] W. Ivison, C. Hambidge, L. Doherty and M. McGilvray, "Commissioning Ludieg Mode with Isentropic Compresssion Heating for the Oxford High Density Tunnel," p. 2755, 2024.

[8] M. McGilvray, L. J. Doherty, A. J. Pearce and P. Ireland, "The Oxford High Density Tunnel," in *20th AIAA international space planes and hypersonic systems and technologies conference*, 2015.

[9] S. Wylie, L. Doherty and M. McGilvray, "Commisioning of the Oxford High Density Tunnel (HDT) for Boundary Layer Stability Measurements at Mach 7," in *2018 Fluid Dynamics Conference*, 2018.

[10] W. Ivison, C. Hambridge, M. McGilvray, A. Flinton, J. Merrifield and J. Steelant, "Heat Flux Augmentation Caused by Surface Imperfections in Turbulent Boundary Layers," in *HiSST: 3rd International Conference on High-Speed Vehicle Science & Technology*, Busan, Korea, 2024.

[11] M. Netterfield, "Validation of a Navier-Stokes code for thermochemical non equillibrium flows," FGE, 1992.

[12] M. Haynes, "ANITA 9.5 Input Manual," FGE, Emsworth, 2024.

[13] E. Toro, M. Spuce and W. Speares, "Restoration of the contact surface in the HLL Riemann solver," Technical report CoA 9204. Department of, Cranfield, UK, 1992.

[14] R. Langtry and F. Menter, "Correlation-Based Transition Modeling for Unstructured Parallelized Computational Fluid Dynamics Codes," *AIAA,* vol. 47, no. 12, pp. 2894-2906, 2009.

[15] F. R. Menter, "Two-equation Eddy-viscosity turbulence models for engineering applications," *AIAA,* pp. 1598-1605, 1994.

[16] F. G. Blottner, M. Johnson and M. Ellis, "Chemically Reacting Viscous Flow Program for Multicomponent Gas Mixtures," Sandia Laboratories Report No SC-RR-70-754, Albuquerque, New-Mexico, 1971.

[17] Cadence, Pointwise, [Online]. Available: https://www.pointwise.com/. [Accessed 7 3 2024].

[18] D. Estruch, D. MacManus, J. Stollery, N. Lawson and K. Garry, "Hypersonic interference Heating in the Vicinity of Surface Protuberances," *Exp. Fluids,* vol. 3, no. 49, pp. 683-699, 2010.